

High-pressure phase transitions of zinc difluoride up to 55 GPa

Dominik Kurzydłowski^{1*}, Anna Oleksiak¹, Sharad Babu Pillai,² Prafulla K. Jha²

¹ Faculty of Mathematics and Natural Sciences, Cardinal Stefan Wyszyński University, Warsaw 01-038, Poland;

² Department of Physics, Faculty of Science, The Maharaja Sayajirao University of Baroda, Vadodara 390002, India

*Correspondence: d.kurzydowski@uksw.edu.pl

Studying the effect of high pressure (exceeding 10 kbar) on the structure of solids allows to gain deeper insight in the mechanism governing crystal structure stability. Here we report a study on the high-pressure behaviour of zinc difluoride (ZnF_2) – an archetypical ionic compound which at ambient pressure adopts the rutile (TiO_2) structure. Previous investigations, limited to a pressure of 15 GPa, revealed that this compound undergoes two pressure-induced phase transitions: $\text{TiO}_2 \rightarrow \text{CaCl}_2$ at 4.5 GPa, and $\text{CaCl}_2 \rightarrow \text{HP-PdF}_2$ at 10 GPa. Within this joint experimental-theoretical study we extend the room-temperature phase diagram of ZnF_2 up to 55 GPa. By means of Raman spectroscopy measurements we identify two new phase transitions: $\text{HP-PdF}_2 \rightarrow \text{HP1-AgF}_2$ at 30 GPa and $\text{HP1-AgF}_2 \rightarrow \text{PbCl}_2$ at 44 GPa. These results are confirmed by Density Functional Theory calculations which indicate that in the HP1-AgF_2 polymorph the coordination sphere of Zn^{2+} undergoes drastic changes upon compression. Our results point to important differences in the high-pressure behaviour of ZnF_2 and MgF_2 , despite the fact that both compounds contain cations of similar size. We also argue that the HP1-AgF_2 structure, previously observed only for AgF_2 , might be observed at large compression in other AB_2 compounds.

Introduction

Rationalizing the crystal structures of solids is an ongoing endeavour in material sciences. Concepts such as the Goldschmidt tolerance factor,¹ Pauling rules,² or the bond-valence index³ are important tools for understanding and predicting crystal geometry. Metal difluorides (MF_2) are an excellent group of compounds for testing these and other concepts.^{4,5} One reason for this is the large variation of the M^{2+} cationic radius which increases from 0.45 Å for Be^{2+} to 1.35 Å for Ba^{2+} (Shannon's effective ionic radius for six-fold coordination, $R_{\text{M}^{2+}}$).⁶ Another important feature of MF_2 systems lies in the range of electronic configurations adopted by M^{2+} cations: for group 2 metals they exhibit a closed-shell, for group 12 and 14 a filled sub-shell (d for group 12, s and d for group 14), while transition metal cations have an open d shell.

In recent years particular attention was drawn to phase transitions of MF_2 compounds induced by pressures exceeding 1 GPa (=10 kbar). Numerous experimental and theoretical investigations were conducted in order to establish the phase sequence for these compounds.⁷⁻²⁵ The motivation for these studies was the fact that the behaviour of difluorides at these conditions can serve as an analogue of

the high-pressure transformations of dioxides, in particular SiO_2 .^{7,8} Moreover high-pressure studies on MF_2 systems revealed a surprisingly wide range of structures adopted by these compounds. At ambient conditions difluorides adopt structures belonging either to the rutile (TiO_2) or fluorite (CaF_2) family, with the exception of BeF_2 and SnF_2 .^{26,27} In contrast, at high pressure the potential energy surface of MF_2 systems is characterized by a number of local minima of similar enthalpy, often separated by large energy barriers.¹⁸

For transition metal difluorides it was found that the high-pressure phase transition sequence differs considerably between ions of similar size, but with different d electron count, as witnessed by comparing MnF_2 (d^5 system)^{8,19} and CoF_2 (d^7 electron count).²⁰ Moreover for d^9 cations (Cu^{2+} , Ag^{2+}) the high-pressure polymorphism is strongly influenced by structural distortion arising from an uneven occupation of the e_g orbitals (often referred to as the Jahn-Teller effect)²⁸ as well as strong spin-spin magnetic interactions.²⁴ In this context the phase transitions of zinc difluoride are of interest, as the Zn^{2+} cation can be viewed as a non-magnetic ($3d^{10}$ electronic configuration) counterpart of Mn^{2+} , Co^{2+} , and Cu^{2+} . Given the similar size of Zn^{2+} and Mg^{2+} ($R_{\text{Zn}^{2+}} = 0.74 \text{ \AA}$, $R_{\text{Mg}^{2+}} = 0.72 \text{ \AA}$) one could expect that the phase transition of ZnF_2 would be similar to those exhibited by MgF_2 .¹⁸ However experimental data for the former compound is only available to a moderate pressure of 15 GPa,^{9,10,25} while theoretical predictions were restricted to pressures not exceeding 12 GPa, and performed taking into account only a limited number of possible structure types.^{11,12}

Here we extend the phase diagram of ZnF_2 to 55 GPa by performing Raman scattering measurements with the use of the diamond anvil cell (DAC). The obtained data confirms the previously reported phase transition from a CaCl_2 -type structure to the HP-PdF₂ polytype at 10.4 GPa.¹⁰ Two additional phase transitions are observed at 30 and 44 GPa. We assign the first of these as a transformation from the HP-PdF₂ polymorph to a non-centrosymmetric structure (space group $Pca2_1$, $Z = 4$) analogous to the high-pressure structure of AgF_2 (HP1-AgF₂ structure type). The second transition at 44 GPa is between HP1-AgF₂ and the cotunnite (PbCl_2) structure. Our results are confirmed by Density Functional Theory (DFT) calculations and evolutionary algorithm structure searches. DFT modelling indicates that upon compression of the HP1-AgF₂ polymorph the coordination sphere of Zn^{2+} smoothly evolves from octahedral to tricapped trigonal prismatic. Our results indicate also important differences in the high-pressure behaviour of MgF_2 and ZnF_2 .

Experimental and computational details

Raman spectroscopy: Raman spectra were acquired at room temperature with the use of the Alpha300M+ confocal microscope (Witec GmbH). We used a 532 nm laser line delivered to the

microscope through a single-mode optical fiber. Laser power at the sample did not exceed 30 mW. The Raman signal was collected through a 20× long working distance objective, and passed through a multi-mode optical fiber (50 μm core diameter) to a lens-based spectrometer (Witec UHTS 300, f/4 aperture, focal length 300 mm) coupled with a back-illuminated Andor iDUS 401 detector thermoelectrically cooled to −60°C. The spectra were collected with the use of a 1800 mm grating resulting in a 1.2 cm^{−1} spectral resolution. Typical acquisition times ranged from 1 to 4 s with 30 to 60 accumulations. The spectra were post-processed (background subtraction and cosmic-ray removal) with the Project FIVE software (Witec GmbH). The position of Raman bands was established with the Fityk 1.3.1 software by fitting the observed bands with Pseudo-Voigt profiles.²⁹

High-pressure experiments: two high-pressure runs were conducted with the use of a SymmDAC diamond anvil cell supplied by Almax easyLab bvba. The DAC was equipped with low-fluorescence Ia diamonds with a 400 μm culet and a stainless-steel gasket pre-indented to a thickness of 35 μm. The gasket hole with a radius of 120 μm was laser-drilled. The hole was filled by zinc difluoride powder (anhydrous, 99% purity, supplied by Thermo Fisher GmbH) after which the cell was closed. The starting pressure of the experiments was 4.5 GPa. The pressure was determined from the shift of the R1 ruby fluorescence line.³⁰ During the experiments the DAC was systematically heated to 100°C in order to minimize deviatoric stress in the sample.

DFT calculations: Periodic DFT calculations of the geometry and enthalpy of various polymorphs of ZnF₂ utilized the SCAN meta-GGA functional.³¹ This functional was found to be superior to both Local Density Approximation (LDA) and Generalized-Gradient Approximation (GGA) functionals in predicting the phase transition pressures for a wide range of compounds.^{32,33} SCAN was also successfully used to model the properties of the high-pressure phases of silver difluoride, AgF₂.²⁴ We found it to reproduce very well the geometry of the previously reported polymorphs of ZnF₂ (see Table S1 in the Supplementary Information, SI). The projector-augmented-wave (PAW) method was used in the calculations,³⁴ as implemented in the VASP 5.4 code.^{35,36} The cut-off energy of the plane waves was set to 800 eV with a self-consistent-field convergence criterion of 10^{−7} eV. Valence electrons (Zn: 3d¹⁰, 4s²; F: 2s², 2p⁵) were treated explicitly, while standard VASP pseudopotentials were used for the description of core electrons. The k-point mesh spacing was set to 2π × 0.03 Å^{−1}. All structures were optimized until the forces acting on the atoms were smaller than 1 meV/Å.

Calculations were performed for 14 structure types listed in Table 1. Additionally we performed evolutionary algorithm searches for lowest-enthalpy structures of ZnF₂. For this we used the XtalOpt

software (version r12)³⁷ coupled with periodic DFT calculations utilizing the PBE functional.³⁸ These searches were conducted at 10/30/80 GPa for $Z = 4$, and 35/50 GPa for $Z = 8$.

Calculations of Γ -point vibration frequencies were conducted in VASP 5.4 utilizing the SCAN functional. The finite-displacement method was used with a 0.025 Å displacement, and a tighter SCF convergence criterion (10^{-8} eV). In case of the HP1-AgF₂, SrI₂, and PbCl₂ structure types we additionally calculated the intensity of Raman-active modes using density-functional perturbation theory (DFPT),³⁹ as implemented in Quantum Espresso code.⁴⁰ The exchange-correlation functional was handled by the LDA approximation of Perdew and Wang.⁴¹ Expansion of wave function and charge density in the plane wave basis set was truncated with energy cut-offs of 110, and 170 Ry for HP1-AgF₂/PbCl₂ and SrI₂ structures, respectively. Brillouin zone was sampled on dense k-mesh ($2\pi \times 0.03 \text{ \AA}^{-1}$) given by the Monkhorst-Pack scheme. Raman activity of phonon modes were determined implementing the second order response method.⁴² We did not apply any scaling of the theoretical vibration frequencies when comparing them with experimental values.

For calculations of the electronic band gap (E_g) of the most stable structure of ZnF₂ we employed the Heyd-Scuseria-Ernzerhof (HSE06) functional,⁴³ which is a hybrid functional mixing the GGA functional of Perdew et al.,³⁸ with 25% of the Hartree-Fock exchange energy. Calculations were performed for the SCAN-relaxed structures. We found that the use of the HSE06 functional for the SCAN geometries results in small forces on atoms ($<0.05 \text{ eV/\AA}$) and moderate residual stress ($<5 \text{ GPa}$).

Visualization of all structures was performed with the VESTA software package.⁴⁴ For symmetry recognition we used the FINDSYM program.⁴⁵ Group theory analysis of the vibrational modes was performed with the use of the Bilbao Crystallographic Server.⁴⁶

Results and discussion

We start by introducing the structure types relevant to this study which we group into four families (see Table 1): rutile, fluorite, zirconia and cotunnite. The structures in the rutile family exhibit octahedral coordination by F⁻ with the coordination number (CN) of the cation equal to 6. At ambient conditions the majority of known metal difluorides adopt the rutile structure (TiO₂, $I4/mmm$, $Z = 2$). Both CrF₂ and CuF₂ adopt a distorted variant of this structure (CuF₂, $P2_1/c$, $Z = 2$) with the first coordination sphere of Cr²⁺/Cu²⁺ in the form of an elongated octahedron (4 + 2 coordination).⁴⁷ The distortion leading to the CuF₂-type structure is a result of a negative force constant for the B_{2g} and B_{3g} vibration modes of the TiO₂ structure.^{48,49} Compression of fluorides exhibiting the TiO₂ structure often

results in a second-order ferroelastic phase transition to an orthorhombic structure (CaCl_2 , $Pnmm$, $Z = 2$), as seen for MgF_2 at 9.1 GPa.¹⁸ This phase, which differs from the TiO_2 polytype by rotation of the MF_6 octahedra along axes parallel to the c lattice vector, retains the coordination environment of M^{2+} . The last member of the rutile family is the $\alpha\text{-PbO}_2$ structure ($Pbcn$, $Z = 4$) which also exhibits octahedral coordination of M^{2+} .

Table 1 Structure types adopted by MF_2 systems together with their space group, number of formula units per cell (Z), and the coordination number of the M^{2+} cation (CN).

Structure family	Structure type	Space group	Z	CN	Comments
Rutile	TiO_2	$P4_2/mnm$	2	6	rutile
	CuF_2	$P2_1/c$	2	4 + 2	distorted TiO_2
	CaCl_2	$Pnmm$	2	6	distorted TiO_2
	$\alpha\text{-PbO}_2$	$Pbcn$	4	6	
Fluorite	CaF_2	$Fm-3m$	4	8	fluorite
	HP-PdF ₂	$Pa-3$	4	6	
	AgF_2	$Pbca$	4	4 + 2	distorted HP-PdF ₂
	HP1-AgF ₂	$Pca2_1$	4	*	distorted AgF_2
Zirconia	ZrO_2	$P2_1/c$	4	7	baddeleyite
	SrI_2	$Pbca$	8	7	brookite , orthorhombic-I
	HS-ZrO ₂	$Pbcm$	4	8	
	HP2-AgF ₂	$Pbcn$	8	4 + 4	distorted HS-ZrO ₂
Cotunnite	PbCl_2	$Pnma$	4	9	cotunnite
	Ni_2In	$P6_3/mmc$	2	11	

* coordination number dependent on pressure (*vide infra*).

The second family of structures is derived from the fluorite polytype (CaF_2 , $Fm-3m$, $Z = 4$). This structure, adopted at ambient conditions by several MF_2 systems (*e.g.* CaF_2 , SrF_2 , and BaF_2), is characterized by an eightfold (cubic) coordination of M^{2+} . In the HP-PdF₂ structure ($Pa-3$, $Z = 4$) the first coordination sphere of the metal is a distorted octahedron and there are two secondary contacts which complete the cubic coordination. This polytype is observed as the high-pressure form of many MF_2 systems that at ambient conditions adopt the TiO_2 structure (*e.g.* MgF_2 has the following phase sequence: $\text{TiO}_2 \xrightarrow{9.1 \text{ GPa}} \text{CaCl}_2 \xrightarrow{14 \text{ GPa}} \text{HP-PdF}_2$).¹⁸ The HP-PdF₂ polytype has the same space group and Wyckoff position sequence as pyrite (FeS_2), but does not exhibit any F-F bonding analogous to S-S bonding present in FeS_2 .

The remaining two polytypes in the fluorite family are connected with the polymorphs of silver difluoride. At ambient conditions this compound adopts a lower-symmetry variant of the HP-PdF₂

structure (AgF_2 , $Pbca$, $Z = 4$) with the first coordination sphere of Ag^{2+} in a form of an elongated octahedron.⁵⁰ This structure transforms at around 9 GPa to a non-centrosymmetric polymorph (HP1- AgF_2 , $Pca2_1$, $Z = 4$).²² The transformation is driven by a phonon instability of the AgF_2 structure.

The third family of structures is derived from the polymorphs of zirconia (ZrO_2). At ambient pressure and temperature the most stable polymorph of this compound has monoclinic symmetry (ZrO_2 , $P2_1/c$, $Z = 4$). In this structure the metal cation is 7-fold coordinate in the form of a monocapped trigonal prism (capping of one of the rectangular faces). There is one longer secondary contact along the other rectangular face of the trigonal prism. Upon compression ZrO_2 transforms into a SrI_2 -type structure ($Pbca$, $Z = 8$) at 10 GPa.⁵¹ This structure retains the monocapped trigonal prism coordination, but with two additional secondary contacts. The phase transition between the ZrO_2 and SrI_2 structure is first order. In a theoretical study a metastable (*i.e.* thermodynamically less stable than the SrI_2 -type structure) high-pressure polymorph of ZrO_2 was proposed which is characterized by $Pbcm$ symmetry and Z equal to 4.⁵² This polymorph results from the pressure-induced symmetrisation of the ZrO_2 -type structure and hence we term it as HS- ZrO_2 . The metal sites in HS- ZrO_2 are 8-fold coordinated in a form of a bicapped trigonal prism (capping at two rectangular faces); there is one additional contact at a longer distance. The last member of the zirconia family is the structure-type derived from the second high-pressure polymorph of AgF_2 (HP2- AgF_2 , $Pbcn$, $Z = 8$) adopted by this compound above 15 GPa.^{21,22} This structure can be viewed as a distorted variant of HS- ZrO_2 with the first coordination sphere split into four shorter and four longer contacts.

All transition metal difluorides that adopt the CaF_2 structure at ambient conditions transform to the cotunnite structure (PbCl_2 , $Pnma$, $Z = 4$) at relatively low pressures (< 10 GPa).^{7,13-16} This structure is characterized by a nine-fold coordination of M^{2+} in the form of a tricapped trigonal prism with the three anions capping the rectangular faces. At higher pressures the PbCl_2 polytype transforms to an Ni_2In structure in which two additional anions enter the coordination sphere of M^{2+} leading to a 11-fold coordination (pentacapped trigonal prism), the highest observed for metal difluorides.⁷

High-pressure Raman scattering

As nearly all of the first-row transition metal difluorides, zinc difluoride (ZnF_2) adopts the TiO_2 structure at ambient conditions.⁵³ Raman measurements on ZnF_2 compressed to 6.5 GPa in a diamond anvil cell (DAC) indicated that this compound undergoes a transformation to the CaCl_2 -type polymorph at 4.5 GPa.⁹ This transition was confirmed by x-ray diffraction measurements which also indicated a second transition to a HP- PdF_2 structure (space group $Pa-3$) commencing at 10 GPa.¹⁰

Upon decompression from 15.3 GPa the HP-PdF₂ polymorph was stable down to 4 GPa. Below this pressure the sample transformed to a mixture of two phases: TiO₂ and α -PbO₂-type.¹⁰

The Raman spectrum of ZnF₂ in the range 4.5 to 10 GPa (Figure 1) is in accordance with that previously measured for the CaCl₂-type polymorph.⁹ From the six Raman-active modes ($2A_g + 2B_{1g} + B_{2g} + B_{3g}$) two modes of A_g symmetry are observed together with a band resulting from the overlap of one of the B_{1g} modes with a B_{2g} and a B_{3g} mode. The assignment of the modes is based on the comparison between the observed band positions and the frequencies of the Raman-active modes calculated with the use of the SCAN functional (see Figure S 1). The one remaining B_{1g} mode, predicted to appear at frequencies above 550 cm⁻¹ is not observed, most probably due to its low intensity.

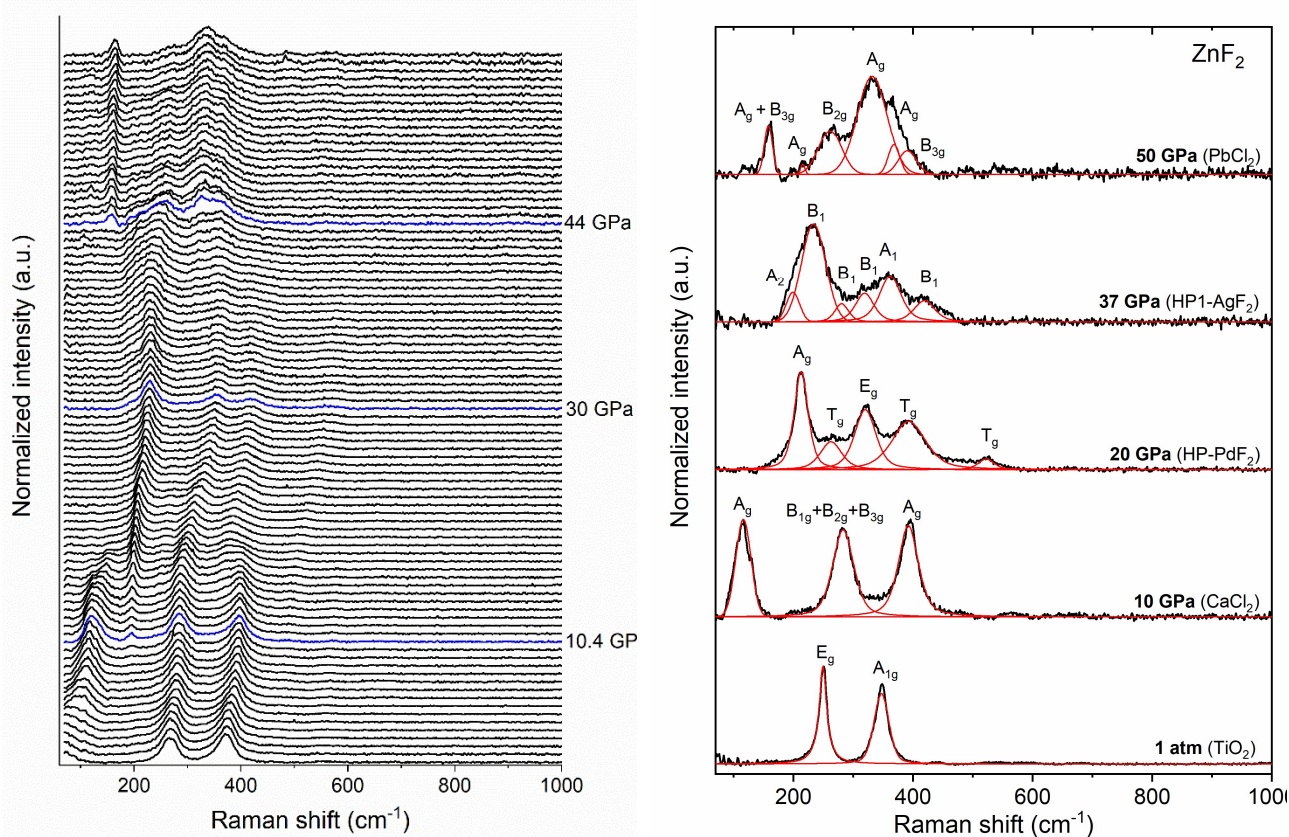


Figure 1 Left: Evolution of the Raman spectrum of powdered ZnF₂ from 4.5 to 55 GPa (the spectra are offset for clarity). Spectra marked in blue are taken at pressures at which phase transitions are observed (10.4, 30 and 40 GPa). **Right:** Raman spectrum of ZnF₂ at selected pressure together with the deconvolution into component functions. Labels denote the symmetry of each mode.

Upon compression of the CaCl₂-type phase all of the observed bands shift to higher wavenumbers (Figure 2), with a particularly large pressure dependence observed for the least energetic A_g transition (Table S 2). At 10.4 GPa a new band appears around 195 cm⁻¹ and upon compression grows in intensity at the expense of the two A_g modes (Figure 1). At the same pressure the band originating from the

$B_{1g}/B_{2g}/B_{3g}$ modes changes its pressure dependence. These changes, together with the appearance of three additional bands (250, 380, and 500 cm^{-1} at 13.5 GPa) mark the gradual transition from the CaCl_2 -type polymorph to the HP-PdF₂ structure. This transition is completed at 15.9 GPa as signalled by the complete disappearance of the bands originating from the CaCl_2 polymorph. The pressure at which the CaCl_2 – HP-PdF₂ transition is observed as well as the coexistence of both phases up to 16 GPa is in accordance with previous x-ray diffraction measurements.¹⁰ We observe all five of the Raman-active modes of the HP-PdF₂ structure ($A_g + E_g + 3T_g$). Thanks to an excellent agreement between measured band position and calculated frequencies of vibrational modes (see Figure S 2) we were able to assign the symmetry of all of these modes.

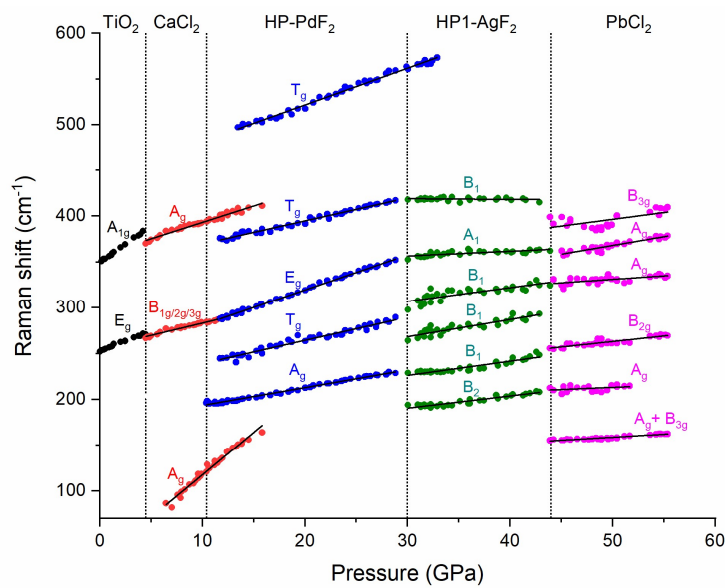


Figure 2 Pressure dependence of the frequencies of Raman bands of ZnF_2 measured upon compression. Points corresponding to the $\text{TiO}_2/\text{CaCl}_2/\text{HP-PdF}_2/\text{HP1-AgF}_2/\text{PbCl}_2$ phases are marked with black/red/blue/green/magenta. Black lines are linear fits (see Table S 2). Data for the TiO_2 polymorph is taken from ref. ⁹.

Compression of the HP-PdF₂ polymorph to 30 GPa leads to a gradual stiffening of all of the observed modes with the highest-frequency T_g mode having the largest pressure coefficient dv/dp (Table S 2). At 30 GPa two shoulders develop on both sides of the A_g band and the intensity of the highest-frequency T_g mode decreases upon compression (Figure 1 and Figure S 3). This is accompanied by a decrease in the dv/dp coefficient for the bands located at 355 and 420 cm^{-1} at 30 GPa, as seen in Figure 2. These gradual transformations point towards a phase transition into a structure resembling the HP-PdF₂ polymorph, but exhibiting lower symmetry. Based on the comparison of calculated and experimental vibration frequencies (Figure S 4) we assign the phase appearing at 30 GPa to the HP1-AgF₂ structure. Of the 33 Raman-active modes present for this non-centrosymmetric structure ($8A_1 + 9A_2 + 8B_1 + 8B_2$) we observe 6 ($A_1 + A_2 + 3B_1$).

The last phase transition is observed at 44 GPa. Its most characteristic feature is the redistribution of intensity of the band observed in the 200 – 400 cm^{-1} region, and the appearance of a band at 150 cm^{-1} whose position varies only slightly with pressure (dv/dp equal to 0.65 $\text{cm}^{-1}/\text{GPa}$). Comparison of the calculated and experimental frequencies of Raman active modes (Figure S 5) indicated that the phase observed above 44 GPa is the PbCl_2 -type (cotunnite) polymorph of ZnF_2 . With the aid of the SCAN calculations we are able to assign the observed Raman bands. From the 18 Raman-active modes ($6A_g + 3B_{1g} + 6B_{2g} + 3B_{3g}$) we observe six ($4A_g + B_{2g} + 2B_{3g}$) with A_g and B_{3g} low-frequency modes coalescing into one band at 150 cm^{-1} . This analysis is corroborated by the good accordance between the experimental spectrum and that simulated for the PbCl_2 polymorph (Figure S 5).

DFT calculations

In order to confirm the nature of the experimentally observed phase transitions we calculated the geometry and enthalpy of various phases of ZnF_2 at pressures up to 100 GPa. For these calculations we assumed the structure types listed Table 1. Additional evolutionary algorithm searches were performed in order to identify other possible high-pressure polymorphs of ZnF_2 (see Materials and Methods). However these searches did not yield any new structures which would be competitive in terms of enthalpy with those listed in Table 1.

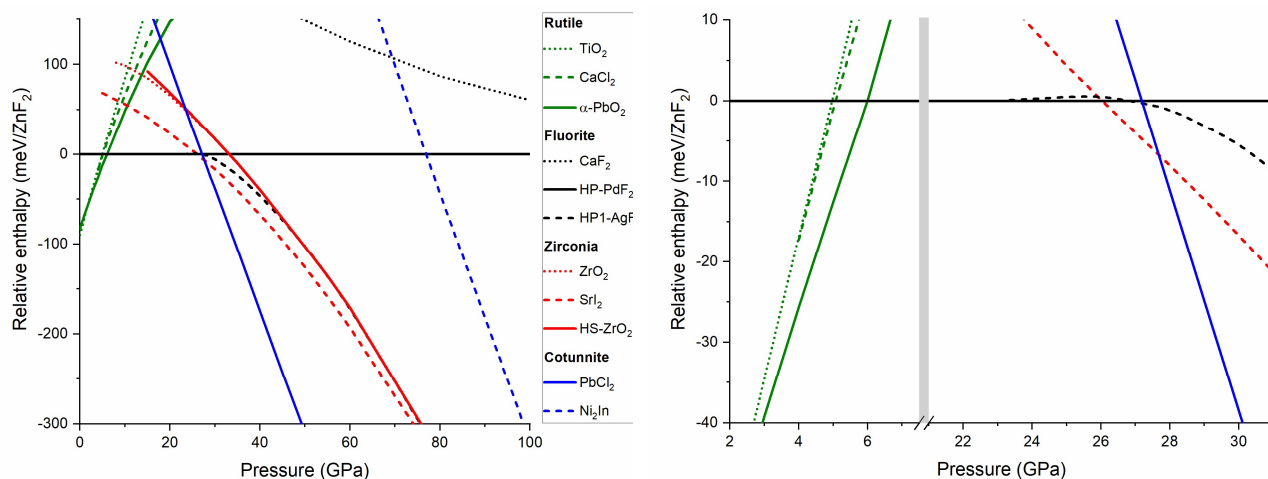


Figure 3 Left: Pressure dependence of the relative enthalpy (referenced to that of the HP-PdF_2 structure) of ZnF_2 polymorphs up to 300 GPa. **Right:** Zoom into the 2 – 7.5 and 21 – 31 GPa region.

Upon geometry optimization the CuF_2 , AgF_2 , and HP2-AgF_2 structure types symmetrized to the TiO_2 , HP-PdF_2 , and HS-ZrO_2 structures, respectively. This is not surprising given that the three former polymorphs are distorted variants of the latter, with the distortions arising from the uneven occupation of the e_g orbitals which is not present for the closed-shell Zn^{2+} cation. Interestingly the

non-centrosymmetric HP1-AgF₂ structure did retain its symmetry upon geometry optimization, although the coordination around the M²⁺ cation changed from 4 + 2 to 6 at 25 GPa.

In accordance with experiment at ambient pressure (effectively 0 GPa) TiO₂ is the most stable structure. Our calculations indicate that this structure should transform into α -PbO₂ at 1.8 GPa. However the α -PbO₂ phase is not observed experimentally. This situation resembles that found in other AB₂ compounds (*e.g.* MgF₂ and SnO₂)^{18,54} for which the α -PbO₂ structure is not observed during compression despite being more stable in calculations than the experimentally observed CaCl₂ structure. This discrepancy was rationalized by taking into account the large energetic barrier associated with the TiO₂ to α -PbO₂ transition.^{18,54} In case of ZnF₂ calculations give the TiO₂ – CaCl₂ transition at 4 GPa (Figure 3) in very good agreement with the experimental value of 4.5 GPa.⁹ The transition from CaCl₂ to HP-PdF₂ is predicted at 5.1 GPa in good agreement with the experimental value (10.4 GPa).

Comparison of the relative enthalpies of ZnF₂ polymorphs indicates that the HP-PdF₂ polymorph remains the most stable structure of ZnF₂ up to a pressure of 26 GPa. Above this pressure the SrI₂ structure type is predicted to be the ground state, but only in a narrow pressure range up to 27.7 GPa. Above this pressure the PbCl₂ (cotunnite) structure has a lower enthalpy and remains the most stable polymorph up to 100 GPa.

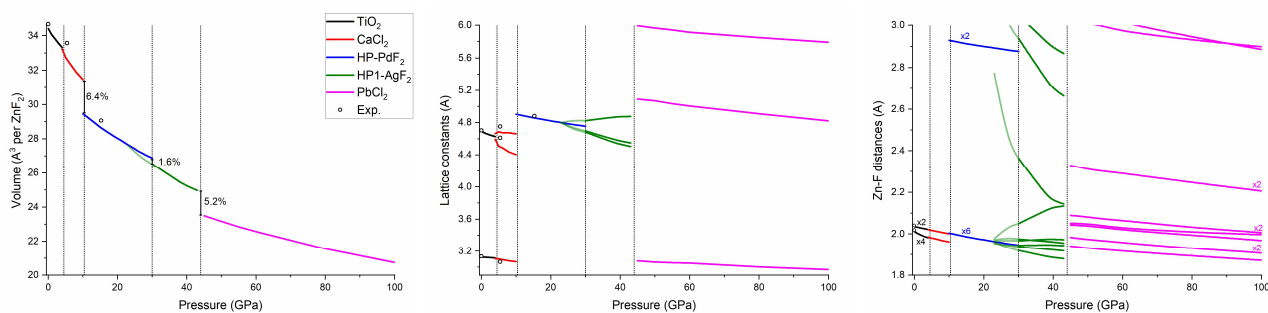


Figure 4 Calculated pressure dependence of the volume (left), lattice constants (middle), and Zn-F distances (right) of the experimentally observed polymorphs of ZnF₂. Dotted vertical lines indicate experimental transition pressures (4.5, 10.4, 30, and 44 GPa). Open circles indicate experimental values.^{10,53}

In experiment we observe that at 30 GPa that HP-PdF₂ transforms to the HP1-AgF₂. The latter structure is indeed more stable than HP-PdF₂ above 26 GPa but in the same pressure regime it is less stable than SrI₂ and PbCl₂ (Figure 3). Comparing the evolution of the cell vectors and Zn-F distances (Figure 4) one can clearly see that orthorhombic HP1-AgF₂ is a distorted variant of the cubic HP-PdF₂. Moreover calculations show that HP1-AgF₂ can be obtained from HP-PdF₂ by following an imaginary Γ -point mode of T_u symmetry which develops in the cubic structure at 32 GPa. Therefore at this pressure the HP1-AgF₂ to HP-PdF₂ transition should be characterized by a very small energetic barrier. In contrast

the transition from HP-PdF₂ to SrI₂ or PbCl₂ is most probably characterized by a large barrier as it requires a change in the geometry around the M²⁺ ion from 6-fold octahedral to 7-fold monocapped trigonal prismatic (SrI₂) or 9-fold tricapped trigonal prismatic (PbCl₂). The existence of a low-energy distortion pathway between HP-PdF₂ and HP1-AgF₂ explains why this transition is observed in the room-temperature experiment. We also note that in case of MgF₂ the SrI₂ phase is also not observed experimentally,¹⁸ although it is predicted to be thermodynamically stable between 40 and 44 GPa.¹⁷

In experiment the metastable HP1-AgF₂ phase is observed up to 44 GPa. At this point it transforms to the PbCl₂ structure. It may be speculated that with the use of high temperatures (T > 1000 K) this transition could be observed at lower pressures. High temperatures could also enable the direct transformation of HP-PdF₂ to PbCl₂, as witnessed in the case of MgF₂.¹⁸ Such experiments would however require laser heating of the sample which is unavailable to us in the current experiment experimental set-up. Our calculations indicate that PbCl₂ should remain the most stable structure up to 350 GPa at which it should transform to the anti-Ni₂In structure which features 11-coordinated Zn²⁺. The large value of the pressure required for the PbCl₂ to anti-Ni₂In transition is consistent with the small radius of Zn²⁺.⁷

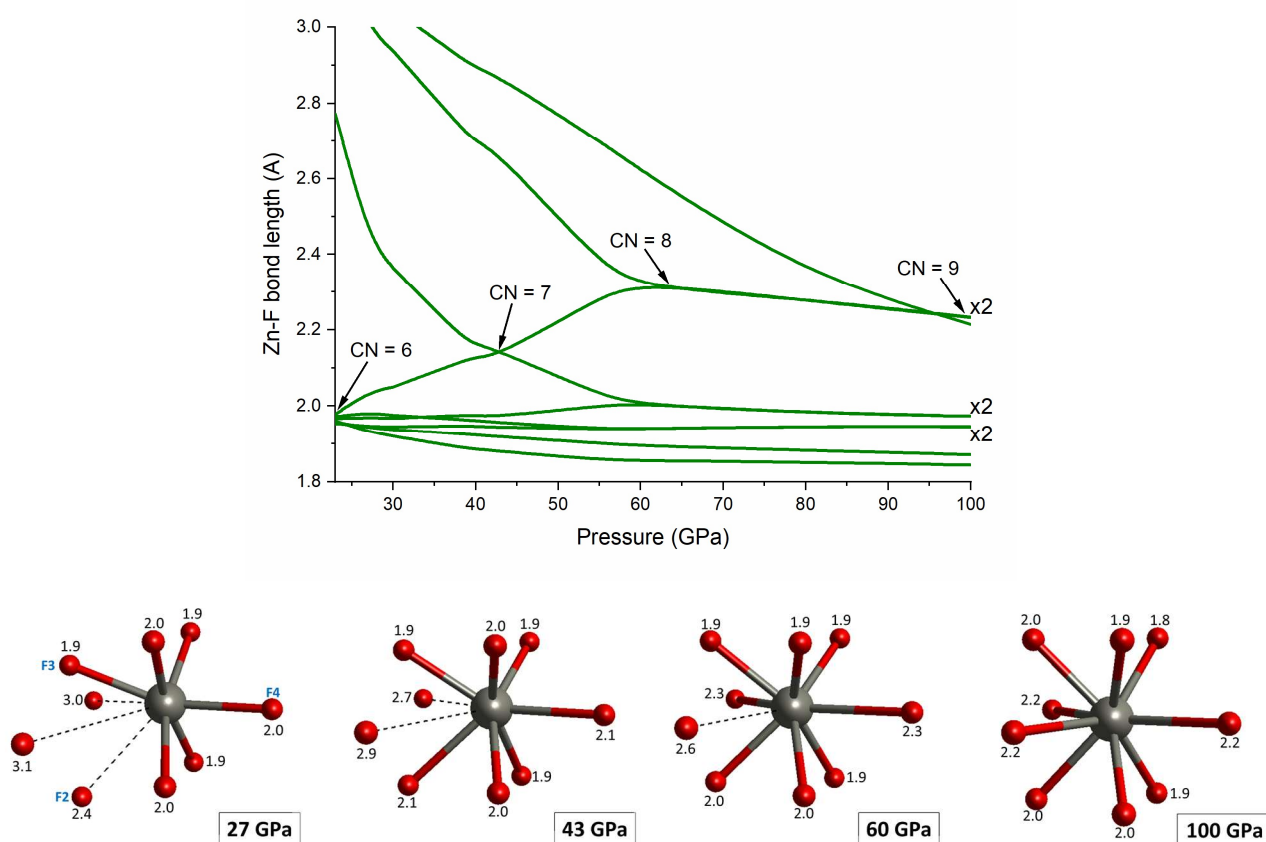


Figure 5 Calculated pressure dependence of the Zn-F distances in the HP1-AgF₂ polymorph of ZnF₂ together with the evolution of the Zn²⁺ coordination sphere in that structure. Distances are given in Å.

Calculations reveal substantial pressure-induced changes in the coordination of Zn^{2+} in the HP1- AgF_2 structure. At 23 GPa the coordination sphere has the form of a distorted octahedron with six Zn-F contact with a distance of around 2 Å. As can be seen in Figure 5 upon compression the F3-Zn-F4 angles strongly deviates from 180° , and the Zn-F4 distances lengthens (nearly 8 % from 23 to 43 GPa). At the same time the secondary Zn-F2 contact shortens considerably (by 23 % from 23 to 43 GPa) and becomes equal in length to Zn-F4 at 43 GPa. These changes mark a gradual transition of the coordination sphere from octahedral (CN = 6) to monocapped trigonal prismatic coordination (CN = 7) which is analogous to that found in the SrI_2 structure (Figure 5). Further compression leads to an increase of the coordination number to 8 at 60 GPa with the coordination sphere in the form of a bicapped trigonal prism. At this pressure HP1- AgF_2 in fact becomes isostructural to HS- ZrO_2 which exhibits the same CN. Further compression leads to one more F^- anion entering the first coordination sphere of Zn^{2+} leading to a tricapped trigonal prismatic coordination (CN = 9) resembling that found for the PbCl_2 structure. The pressure-induced changes in the Zn-F distances in the HP1- AgF_2 polymorph (especially the lengthening of the Zn-F4 contact by 18 % from 23 to 60 GPa) points to a surprisingly large plasticity of the Zn^{2+} coordination sphere resembling that found at ambient condition only for compounds containing Jahn-Teller active cations, such as Cu^{2+} and Ag^{2+} .^{55,56}

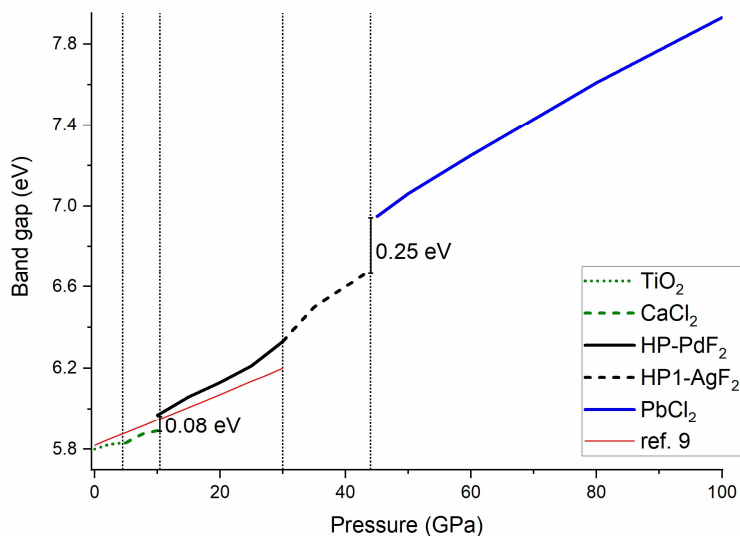


Figure 6 The calculated electronic band gap of the experimentally observed phases of ZnF_2 . Red line indicates values obtained for $\text{TiO}_2/\text{CaCl}_2/\text{HP-PdF}_2$ phases from GGA calculations of ref. ¹¹ (these values are shifted by 2.2 eV for clarity). Dotted vertical lines indicate experimental transition pressures (4.5, 10.4, 30, and 44 GPa).

Calculations of the band gap of ZnF_2 in the TiO_2 structure give the value of 5.8 eV at ambient pressure. This number is smaller than the experimental value (7 – 8 eV)⁵⁷ but larger than those obtained in GGA-based calculations (3.60 – 3.65 eV).^{11,58,59} For all stable ZnF_2 polymorphs compression leads to an

increase in the band gap, but the pressure coefficient (dE_g/dp) differs between phases. For rutile structures (TiO_2 , CaCl_2) it is equal to about 9 meV/GPa, while it is larger for the fluorite structures (21 meV/GPa) and PbCl_2 (18 meV/GPa). These values are larger than reported for CoF_2 ($dE_g/dp < 7$ meV/GPa),²⁰ but smaller than for MgF_2 ($dE_g/dp \approx 40$ meV/GPa).¹⁷ These differences most likely stem from the different electronic configuration between Zn^{2+} ($3d^{10}$), Co^{2+} ($3d^7$) and Mg^{2+} ($2s^2 2p^6$).

Comparison of the calculated phase transition sequence for ZnF_2 and MgF_2 (ref. ¹⁷) show that for the latter compound transition pressures are shifted to higher values. This trend, which is also found when comparing experimental data,¹⁸ can be explained by the smaller radius of Mg^{2+} ($R_{\text{Mg}^{2+}} = 0.72 \text{ \AA}$ vs. $R_{\text{Zn}^{2+}} = 0.74 \text{ \AA}$). A more detailed comparison of the enthalpies of the high-pressure polymorphs reveals that for MgF_2 the HP-PdF₂ and SrI₂ polymorphs are more stable with respect to HP1-AgF₂ and PbCl_2 than for ZnF_2 (Figure 7). This difference may also be a manifestation of the different electronic structure of the cation – a notion that might be explored in future studies. The fact that for the MgF_2 HP1-AgF₂ is less competitive in term of enthalpy explains why this polymorph is not observed experimentally for this compound. We also note that when moving from ZnF_2 to CuF_2 , which contains the Jahn-Teller active Cu^{2+} cation ($3d^9$), the HP1-AgF₂ becomes even more stabilized, and is predicted to be the ground state structure of CuF_2 in a wide pressure range (30 – 72 GPa).²³

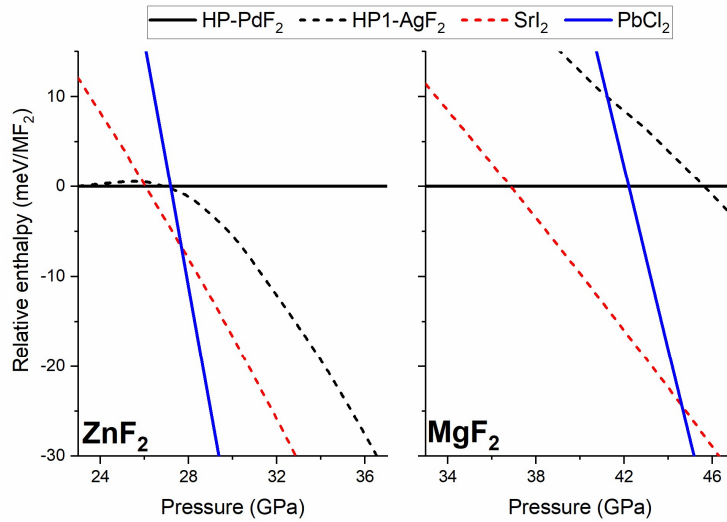


Figure 7 Comparison of the relative enthalpies of the HP-PdF₂, HP1-AgF₂, SrI₂ and PbCl_2 -type structure for ZnF_2 and MgF_2 calculated with the SCAN functional. Both graphs show a pressure interval of 14 GPa and a enthalpy window of 45 meV per MF₂.

Conclusions

In summary high-pressure Raman scattering experiments conducted for ZnF_2 revealed two new phase transition: to the HP1-AgF₂ structure (space group $Pca2_1$) at 30 GPa, and to the PbCl_2 (cotunnite)

polymorph at 44 GPa. The phase transition sequence observed for ZnF_2 is confirmed by DFT calculations which also unveil that the HP1- AgF_2 polymorph is metastable and is formed upon compression from the HP- PdF_2 phase through a phonon instability. The coordination sphere of Zn^{2+} on the non-centrosymmetric HP1- AgF_2 structure changes substantially upon compression smoothly evolving from a cation coordination number of 6 to 9. Comparison of the calculated band gaps and relative phase stability between MgF_2 and ZnF_2 unearths important differences between these systems despite the nearly identical radius of Mg^{2+} and Zn^{2+} .

The observation of the HP1- AgF_2 might have important implications for the study of the phase transition of other AB_2 compounds. We note that the cell vectors of this structure are close to being tetragonal (Figure 4) and therefore HP1- AgF_2 could be considered as a candidate phase for the tetragonal distorted fluorite phase of CoF_2 .²⁰ HP1- AgF_2 exhibits a very similar x-ray diffraction pattern as SrI_2 (see Figure S 6 in SI) and therefore could be taken into account in the analysis of phase transition of compounds for which the SrI_2 phase is observed, such as MnF_2 or PbO_2 .^{19,60,61} Finally we note that despite the similarity of diffraction patterns the Raman spectrum of HP1- AgF_2 and SrI_2 are quite different (Figure S 7) which highlight the usefulness of Raman scattering as a tool for distinguishing different polymorphs of ionic compounds.

Acknowledgments: This research was carried out with the support of the Interdisciplinary Centre for Mathematical and Computational Modelling (ICM), University of Warsaw, under grant no. GB74-8. We thank Marek Tkacz for making available the laser drilling system at the Institute of Physical Chemistry of the Polish Academy of Sciences.

Notes: The authors declare no competing financial interest.

Supporting Information: (i) Comparison of calculated and experimental geometry of the TiO_2 , CaCl_2 , and HP- PdF_2 polymorphs of ZnF_2 ; (ii) Coefficients of the linear fits to the pressure dependence of the frequencies of the Raman-active vibrations; (iii) Comparison of the experimental Raman band position for the CaCl_2 , HP- PdF_2 , HP1- AgF_2 , and PbCl_2 phases of ZnF_2 ; (iv) Evolution of the Raman spectrum of powdered ZnF_2 across the HP- PdF_2 to HP1- AgF_2 transition; (v) Comparison of the experimental Raman spectrum of ZnF_2 at 55 GPa with that simulated with LDA for the PbCl_2 polymorph; (vi) Comparison of the x-ray diffraction pattern simulated for HP1- AgF_2 and SrI_2 structures optimized at 35 GPa; (vii) Comparison of the Raman spectrum simulated for HP1- AgF_2 and SrI_2 optimized at 35 GPa; (viii) Calculated crystal structure of the HP1- AgF_2 polymorph of ZnF_2 at 35 GPa (in VASP format).

References

- (1) Goldschmidt, V. M. No Title. *Naturwissenschaften* **1926**, *14*, 477–485.
- (2) Pauling, L. The Principles Determining the Structure of Complex Ionic Crystals. *J. Am. Chem. Soc.* **1929**, *51*, 1010–1026.
- (3) Brown, I. D. Bond Valences—a Simple Structural Model for Inorganic Chemistry. *Chem. Soc. Rev.* **1978**, *7*, 359.
- (4) García-Fernández, P.; Moreno, M.; Aramburu, J. A. Electrostatic Control of Orbital Ordering in Noncubic Crystals. *J. Phys. Chem. C* **2014**, *118*, 7554–7561.
- (5) Barreda-Argüeso, J. A.; Aguado, F.; González, J.; Valiente, R.; Nataf, L.; Sanz-Ortiz, M. N.; Rodríguez, F. Crystal-Field Theory Validity Through Local (and Bulk) Compressibilities in CoF_2 and KCoF_3 . *J. Phys. Chem. C* **2016**, *120*, 18788–18793.
- (6) Shannon, R. D. Revised Effective Ionic Radii and Systematic Studies of Interatomic Distances in Halides and Chalcogenides. *Acta Crystallogr. Sect. A* **1976**, *32*, 751–767.
- (7) Dorfman, S. M.; Jiang, F.; Mao, Z.; Kubo, A.; Meng, Y.; Prakapenka, V. B.; Duffy, T. S. Phase Transitions and Equations of State of Alkaline Earth Fluorides CaF_2 , SrF_2 , and BaF_2 to Mbar Pressures. *Phys. Rev. B* **2010**, *81*, 174121.
- (8) Stavrou, E.; Yao, Y.; Goncharov, A. F.; Konôpková, Z.; Raptis, C. High-Pressure Structural Study of MnF_2 . *Phys. Rev. B* **2016**, *93*, 054101.
- (9) Perakis, A.; Lampakis, D.; Boulmetis, Y. C.; Raptis, C. High-Pressure Raman Study of the Ferroelastic Rutile-to- CaCl_2 Phase Transition in ZnF_2 . *Phys. Rev. B* **2005**, *72*, 144108.
- (10) Kusaba, K.; Kikegawa, T. In Situ X-Ray Observation of Phase Transitions in ZnF_2 under High Pressure and High Temperature. *Solid State Commun.* **2008**, *145*, 279–282.
- (11) Wu, X.; Wu, Z. Theoretical Calculations of the High-Pressure Phases of ZnF_2 and CdF_2 . *Eur. Phys. J. B* **2006**, *50*, 521–526.
- (12) Torabi, S.; Hammerschmidt, L.; Voloshina, E.; Paulus, B. Ab Initio Investigation of Ground-State Properties of Group-12 Fluorides. *Int. J. Quantum Chem.* **2014**, *114*, 943–951.
- (13) Liu, G.; Wang, H.; Ma, Y.; Ma, Y. Phase Transition of Cadmium Fluoride under High Pressure. *Solid State Commun.* **2011**, *151*, 1899–1902.

- (14) Stan, C. V.; Dutta, R.; White, C. E.; Prakapenka, V. B.; Duffy, T. S. High-Pressure Polymorphism of PbF_2 to 75 GPa. *Phys. Rev. B* **2016**, *94*, 024104.
- (15) Schyck, S.; Evlyukhin, E.; Kim, E.; Pravica, M. G. High Pressure Behavior of Mercury Difluoride (HgF_2). *Chem. Phys. Lett.* **2019**, *724*, 35–41.
- (16) Leger, J. M.; Haines, J.; Atouf, A.; Schulte, O.; Hull, S. High-Pressure x-Ray- and Neutron-Diffraction Studies of BaF_2 : An Example of a Coordination Number of 11 in AX_2 Compounds. *Phys. Rev. B* **1995**, *52*, 13247–13256.
- (17) Nelson, J. R.; Needs, R. J.; Pickard, C. J. High-Pressure Phases of Group-II Difluorides: Polymorphism and Superionicity. *Phys. Rev. B* **2017**, *95*, 054118.
- (18) Haines, J.; Léger, J. M.; Gorelli, F.; Klug, D. D.; Tse, J. S.; Li, Z. Q. X-Ray Diffraction and Theoretical Studies of the High-Pressure Structures and Phase Transitions in Magnesium Fluoride. *Phys. Rev. B* **2001**, *64*, 134110.
- (19) López-Moreno, S.; Romero, A. H.; Mejía-López, J.; Muñoz, A. First-Principles Study of Pressure-Induced Structural Phase Transitions in MnF_2 . *Phys. Chem. Chem. Phys.* **2016**, *18*, 33250–33263.
- (20) Barreda-Argüeso, J. A.; López-Moreno, S.; Sanz-Ortiz, M. N.; Aguado, F.; Valiente, R.; González, J.; Rodríguez, F.; Romero, A. H.; Muñoz, A.; Nataf, L.; et al. Pressure-Induced Phase-Transition Sequence in CoF_2 : An Experimental and First-Principles Study on the Crystal, Vibrational, and Electronic Properties. *Phys. Rev. B* **2013**, *88*, 214108.
- (21) Grzelak, A.; Gawraczyński, J.; Jaroń, T.; Kurzydłowski, D.; Mazej, Z.; Leszczyński, P. J.; Prakapenka, V. B.; Derzsi, M.; Struzhkin, V. V.; Grochala, W. Metal Fluoride Nanotubes Featuring Square-Planar Building Blocks in a High-Pressure Polymorph of AgF_2 . *Dalt. Trans.* **2017**, *46*, 14742–14745.
- (22) Grzelak, A.; Gawraczyński, J.; Jaroń, T.; Kurzydłowski, D.; Budzianowski, A.; Mazej, Z.; Leszczyński, P. J.; Prakapenka, V. B.; Derzsi, M.; Struzhkin, V. V.; et al. High-Pressure Behavior of Silver Fluorides up to 40 GPa. *Inorg. Chem.* **2017**, *56*, 14651–14661.
- (23) Kurzydłowski, D. The Jahn-Teller Distortion at High Pressure: The Case of Copper Difluoride. *Crystals* **2018**, *8*, 140.
- (24) Kurzydłowski, D.; Derzsi, M.; Barone, P.; Grzelak, A.; Struzhkin, V. V.; Lorenzana, J.; Grochala, W. Dramatic Enhancement of Spin–Spin Coupling and Quenching of Magnetic

- Dimensionality in Compressed Silver Difluoride. *Chem. Commun.* **2018**, *54*, 10252–10255.
- (25) Ming, L. C.; Manghnani, M. H.; Matsui, T.; Jamieson, J. C. Phase Transformations and Elasticity in Rutile-Structured Difluorides and Dioxides. *Phys. Earth Planet. Inter.* **1980**, *23*, 276–285.
- (26) McDonald, R. C.; Hau, H. H. K.; Eriks, K. Crystallographic Studies of Tin(II) Compounds. I. Crystal Structure of Tin(II) Fluoride, SnF₂. *Inorg. Chem.* **1976**, *15*, 762–765.
- (27) Ghalsasi, P.; Ghalsasi, P. S. Single Crystal X-Ray Structure of BeF₂ : α -Quartz. *Inorg. Chem.* **2011**, *50*, 86–89.
- (28) Aramburu, J. A.; García-Fernández, P.; Mathiesen, N. R.; Garcia-Lastra, J. M.; Moreno, M. Changing the Usual Interpretation of the Structure and Ground State of Cu²⁺ -Layered Perovskites. *J. Phys. Chem. C* **2018**, *122*, 5071–5082.
- (29) Wojdyr, M. Fityk : A General-Purpose Peak Fitting Program. *J. Appl. Crystallogr.* **2010**, *43*, 1126–1128.
- (30) Dewaele, A.; Torrent, M.; Loubeyre, P.; Mezouar, M. Compression Curves of Transition Metals in the Mbar Range: Experiments and Projector Augmented-Wave Calculations. *Phys. Rev. B* **2008**, *78*, 104102.
- (31) Sun, J.; Ruzsinszky, A.; Perdew, J. P. Strongly Constrained and Appropriately Normed Semilocal Density Functional. *Phys. Rev. Lett.* **2015**, *115*, 036402.
- (32) Hinuma, Y.; Hayashi, H.; Kumagai, Y.; Tanaka, I.; Oba, F. Comparison of Approximations in Density Functional Theory Calculations: Energetics and Structure of Binary Oxides. *Phys. Rev. B* **2017**, *96*, 094102.
- (33) Shahi, C.; Sun, J.; Perdew, J. P. Accurate Critical Pressures for Structural Phase Transitions of Group IV, III-V, and II-VI Compounds from the SCAN Density Functional. *Phys. Rev. B* **2018**, *97*, 94111.
- (34) Blöchl, P. E. Projector Augmented-Wave Method. *Phys. Rev. B* **1994**, *50*, 17953–17979.
- (35) Kresse, G.; Furthmüller, J. Efficient Iterative Schemes for Ab Initio Total-Energy Calculations Using a Plane-Wave Basis Set. *Phys. Rev. B* **1996**, *54*, 11169–11186.
- (36) Kresse, G.; Joubert, D. From Ultrasoft Pseudopotentials to the Projector Augmented-Wave Method. *Phys. Rev. B* **1999**, *59*, 1758–1775.

- (37) Avery, P.; Toher, C.; Curtarolo, S.; Zurek, E. XtalOpt Version R12: An Open-Source Evolutionary Algorithm for Crystal Structure Prediction. *Comput. Phys. Commun.* **2019**, *237*, 274–275.
- (38) Perdew, J. P.; Burke, K.; Ernzerhof, M. Generalized Gradient Approximation Made Simple. *Phys. Rev. Lett.* **1996**, *77*, 3865–3868.
- (39) Baroni, S.; de Gironcoli, S.; Dal Corso, A.; Giannozzi, P. Phonons and Related Crystal Properties from Density-Functional Perturbation Theory. *Rev. Mod. Phys.* **2001**, *73*, 515–562.
- (40) Giannozzi, P.; Baroni, S.; Bonini, N.; Calandra, M.; Car, R.; Cavazzoni, C.; Ceresoli, D.; Chiarotti, G. L.; Cococcioni, M.; Dabo, I.; et al. QUANTUM ESPRESSO: A Modular and Open-Source Software Project for Quantum Simulations of Materials. *J. Phys. Condens. Matter* **2009**, *21*, 395502.
- (41) Perdew, J. P.; Wang, Y. Accurate and Simple Analytic Representation of the Electron-Gas Correlation Energy. *Phys. Rev. B* **1992**, *45*, 13244–13249.
- (42) Lazzeri, M.; Mauri, F. First-Principles Calculation of Vibrational Raman Spectra in Large Systems: Signature of Small Rings in Crystalline SiO₂. *Phys. Rev. Lett.* **2003**, *90*, 036401.
- (43) Krukau, A. V.; Vydrov, O. A.; Izmaylov, A. F.; Scuseria, G. E. Influence of the Exchange Screening Parameter on the Performance of Screened Hybrid Functionals. *J. Chem. Phys.* **2006**, *125*, 224106–1.
- (44) Momma, K.; Izumi, F. VESTA 3 for Three-Dimensional Visualization of Crystal, Volumetric and Morphology Data. *J. Appl. Crystallogr.* **2011**, *44*, 1272–1276.
- (45) Stokes, H. T.; Hatch, D. M. FINDSYM: Program for Identifying the Space-Group Symmetry of a Crystal. *J. Appl. Crystallogr.* **2005**, *38*, 237–238.
- (46) Kroumova, E.; Aroyo, M. I.; Perez-Mato, J. M.; Kirov, A.; Capillas, C.; Ivantchev, S.; Wondratschek, H. Bilbao Crystallographic Server: Useful Databases and Tools for Phase-Transition Studies. *Phase Transitions* **2003**, *76*, 155–170.
- (47) Chatterji, T.; Hansen, T. C. Magnetoelastic Effects in Jahn–Teller Distorted CrF₂ and CuF₂ Studied by Neutron Powder Diffraction. *J. Phys. Condens. Matter* **2011**, *23*, 276007.
- (48) Aramburu, J. A.; Moreno, M. Understanding the Structure and Ground State of the Prototype CuF₂ Compound Not Due to the Jahn–Teller Effect. *Inorg. Chem.* **2019**, *58*, 4609–4618.

- (49) Aramburu, J. A.; Moreno, M. Explaining the Optical Spectrum of CrF₂ and CuF₂ Model Materials: Role of the Tetragonal to Monoclinic Instability. *Phys. Chem. Chem. Phys.* **2019**, *21*, 11714–11723.
- (50) Fischer, P.; Roult, G.; Schwarzenbach, D. Crystal and Magnetic Structure of Silver Difluoride-II. Weak 4d-Ferromagnetism of AgF₂. *J. Phys. Chem. Solids* **1971**, *32*, 1641–1647.
- (51) Leger, J. M.; Tomaszewski, P. E.; Atouf, A.; Pereira, A. S. Pressure-Induced Structural Phase Transitions in Zirconia under High Pressure. *Phys. Rev. B* **1993**, *47*, 14075–14083.
- (52) Öztürk, H.; Durandurdu, M. High-Pressure Phases of ZrO₂: An Ab Initio Constant-Pressure Study. *Phys. Rev. B* **2009**, *79*, 134111.
- (53) O'Toole, N. J.; Streltsov, V. A. Synchrotron X-Ray Analysis of the Electron Density in CoF₂ and ZnF₂. *Acta Crystallogr. Sect. B Struct. Sci.* **2001**, *57*, 128–135.
- (54) Haines, J.; Léger, J. X-Ray Diffraction Study of the Phase Transitions and Structural Evolution of Tin Dioxide at High Pressure: Relationships between Structure Types and Implications for Other Rutile-Type Dioxides. *Phys. Rev. B - Condens. Matter Mater. Phys.* **1997**, *55*, 11144–11154.
- (55) Gažo, J.; Bersuker, I. B.; Garaj, J.; Kabešová, M.; Kohout, J.; Langfelderová, H.; Melník, M.; Serator, M.; Valach, F. Plasticity of the Coordination Sphere of Copper(II) Complexes, Its Manifestation and Causes. *Coord. Chem. Rev.* **1976**, *19*, 253–297.
- (56) Mazej, Z.; Kurzydłowski, D.; Grochala, W. Unique Silver(II) Fluorides: The Emerging Electronic and Magnetic Materials. In *Photonic and Electronic Properties of Fluoride Materials*; Tressaud, A., Poeppelmeier, K., Eds.; Elsevier: Amsterdam, 2016; pp 231–260.
- (57) Nakanishi, Y.; Naito, S.; Nakamura, T.; Hatanaka, Y.; Shimaoka, G. The Influence of Residual O₂ Gas in Vacuum on the Structural and Luminescent Properties of ZnF₂:Mn Thin Films. *Appl. Surf. Sci.* **1996**, *92*, 400–403.
- (58) Wang, L.; Yuan, P.-F.; Wang, F.; Sun, Q.; Liang, E.-J.; Jia, Y. Theoretical Study of Negative Thermal Expansion Mechanism of ZnF₂. *Mater. Res. Bull.* **2012**, *47*, 1113–1118.
- (59) Wu, J.-B.; Cheng, X.-L.; Zhang, H.; Xiong, Z.-W. First-Principles Study of Structural, Electronic and Optical Properties of ZnF₂. *Chinese Phys. B* **2014**, *23*, 077102.
- (60) Haines, J.; Léger, J. M.; Schulte, O. The High-Pressure Phase Transition Sequence from the

Rutile-Type through to the Cotunnite-Type Structure in PbO₂. *J. Phys. Condens. Matter* **1996**, *8*, 1631–1646.

- (61) Grocholski, B.; Shim, S.-H.; Cottrell, E.; Prakapenka, V. B. Crystal Structure and Compressibility of Lead Dioxide up to 140 GPa. *Am. Mineral.* **2014**, *99*, 170–177.

Supplementary Information

Table S 1 Comparison of calculated and experimental geometry of the TiO₂, CaCl₂, and HP-PdF₂ polymorphs of ZnF₂ at selected pressures. Length of unit cell vectors (*a*, *b*, *c*) is given in Å, cell volume (*V*) in Å³. Relative difference between experimental and theoretical values is given in parenthesis.

Structure type	a	b	c	V	Ref.
TiO ₂ p = 1 atm	4.704		3.134	69.33	Exp. ⁵³
	4.694 (-0.2 %)		3.122 (-0.2 %)	68.81 (-0.8 %)	This work
	4.712 (0.2 %)		3.179 (1.4 %)	70.58 (1.8 %)	Calc. ⁵⁹
CaCl ₂ p = 5.4 GPa	4.612	4.751	3.065	67.16	Exp. ¹⁰
	4.683 (1.5 %)	4.502 (-5.2 %)	3.097	65.30 (-2.8)	This work
HP-PdF ₂ p = 15.3 GPa		4.881		116.29	Exp. ¹⁰
		4.857 (-0.6 %)		114.58 (-1.5 %)	This work

Table S 2 Coefficients of the linear fits to the pressure dependence of the frequencies of the Raman-active vibrations.

Phase	Mode symmetry	dv/dp (cm ⁻¹ /GPa)	v _{0GPa} (cm ⁻¹)
CaCl ₂	A _g	3.6(1)	357(1)
	B _{1g} + B _{2g} + B _{3g}	2.7(1)	256(1)
	A _g	9.3(2)	25(3)
HP-PdF ₂	T _g	4.02(6)	441(1)
	T _g	2.50(6)	344(1)
	E _g	3.81(3)	243(1)
	T _g	2.53(8)	214(2)
	A _g	1.93(3)	174(1)
HP1-AgF ₂	B ₁	-0.08(8)	421(3)
	A ₁	0.51(8)	341(3)
	B ₁	1.5(2)	262(7)
	B ₁	1.9(2)	212(6)
	B ₁	1.5(1)	180(4)
	A ₂	1.33(8)	151(3)
PbCl ₂	B _{3g}	1.5(4)	323(19)
	A _g	0.8(2)	293(9)
	A _g	1.9(1)	273(7)
	B _{2g}	1.2(1)	203(6)
	A _g	0.5(3)	190(13)
	A _g + B _{3g}	0.65(4)	126(2)

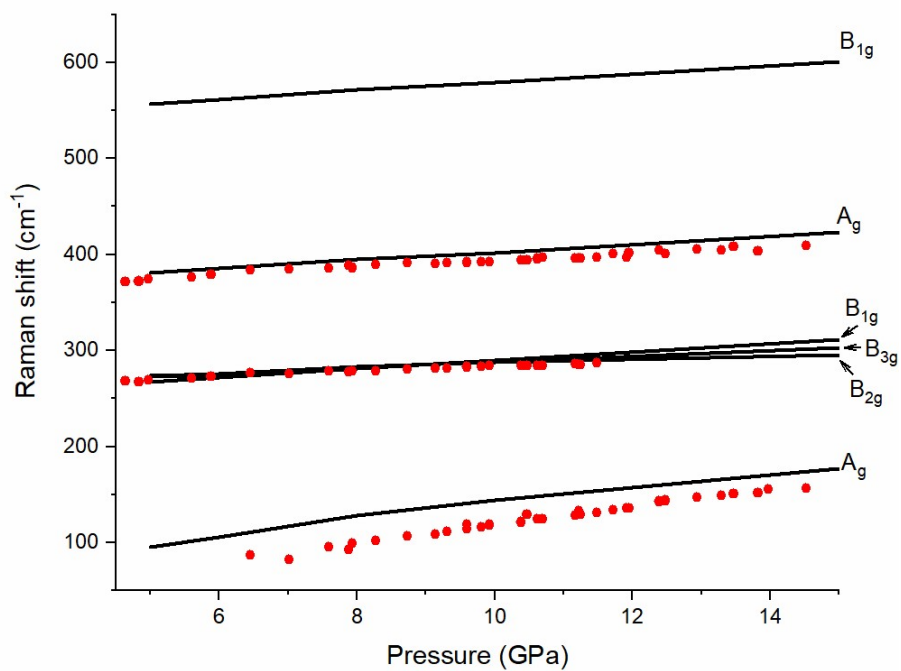


Figure S 1 Comparison of the experimental Raman band position for the CaCl₂-type phase of ZnF₂ (red dots) with the frequencies of Raman-active Γ -point modes calculated for this polymorph using the SCAN functional (black lines). Labels denote the symmetry of each mode.

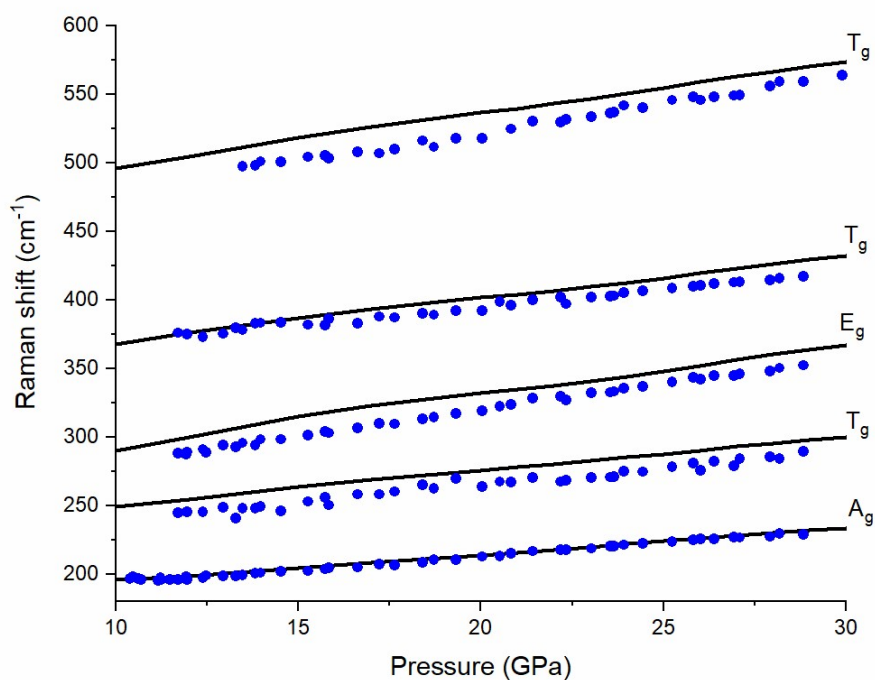


Figure S 2 Comparison of the experimental Raman band position for the HP-PdF₂ phase of ZnF₂ (blue dots) with the frequencies of Raman-active Γ -point modes calculated for this polymorph using the SCAN functional (black lines). Labels denote the symmetry of each mode.

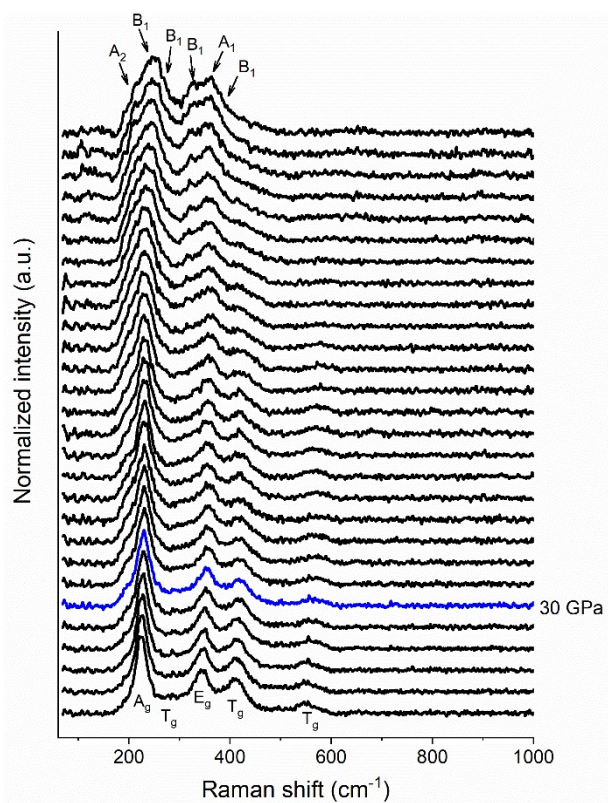


Figure S 3 Evolution of the Raman spectrum of powdered ZnF_2 across the HP-PdF₂ to HP1-AgF₂ transition (26 to 43 GPa). Labels for the Raman bands of HP-PdF₂ (bottom) and HP1-AgF₂ (top) are given. The spectra are offset for clarity.

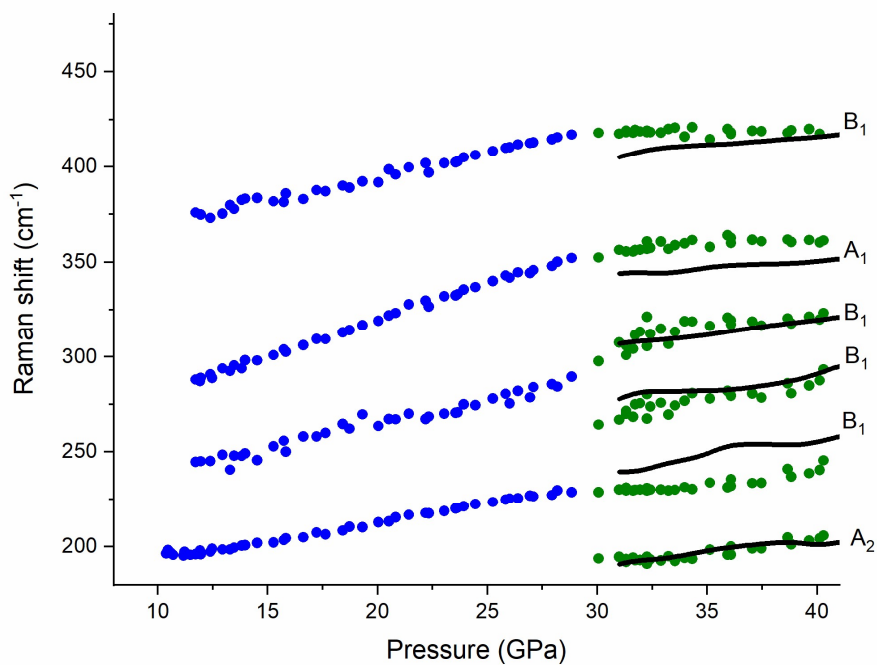


Figure S 4 Comparison of the experimental Raman band position for the HP-PdF₂ and HP1-AgF₂ phases of ZnF_2 (blue and green dots) with the frequencies of selected Raman-active Γ -point modes calculated for HP1-AgF₂ polymorph using the SCAN functional (black lines). Labels denote the symmetry of each mode.

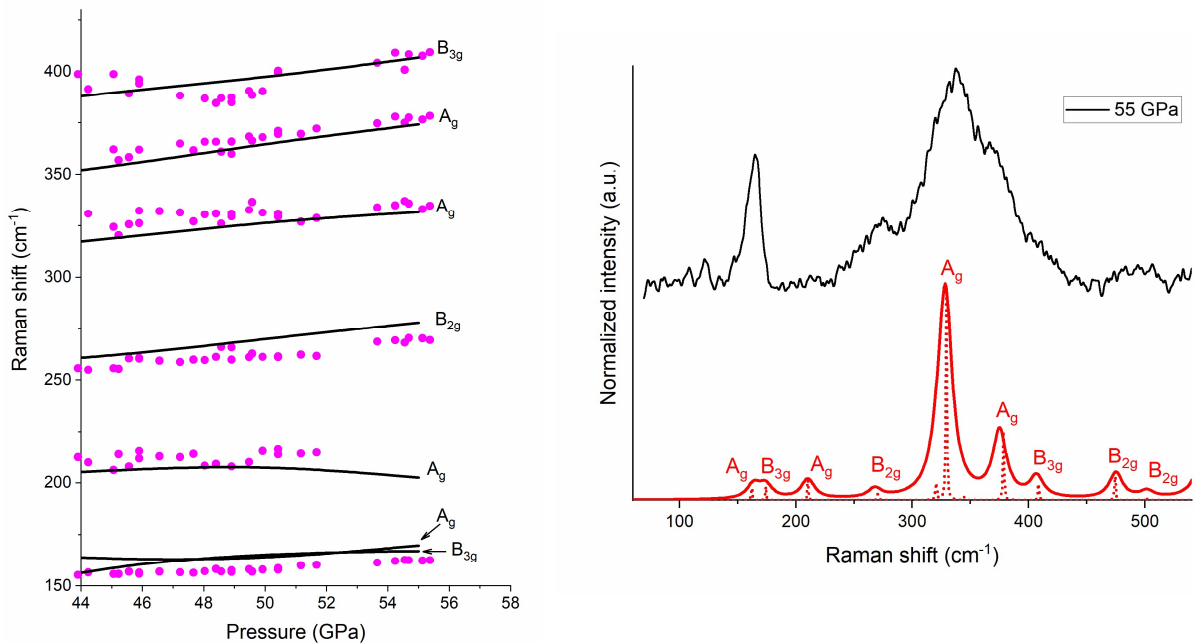


Figure S 5 Left: Comparison of the experimental Raman band position for the PbCl_2 phase of ZnF_2 (magenta dots) with the frequencies of the most intense Raman-active modes calculated for this polymorph using the SCAN functional (black lines). Labels denote the symmetry of each mode. **Right:** Comparison of the experimental Raman spectrum of ZnF_2 at 55 GPa with that simulated with LDA for the PbCl_2 polymorph. Red line denotes the spectrum simulated with a Lorentzian profile characterized by a full width at half maximum (FWHM) of 15 cm^{-1} . The dotted lines correspond to profiles with FWHM equal to 1 cm^{-1} .

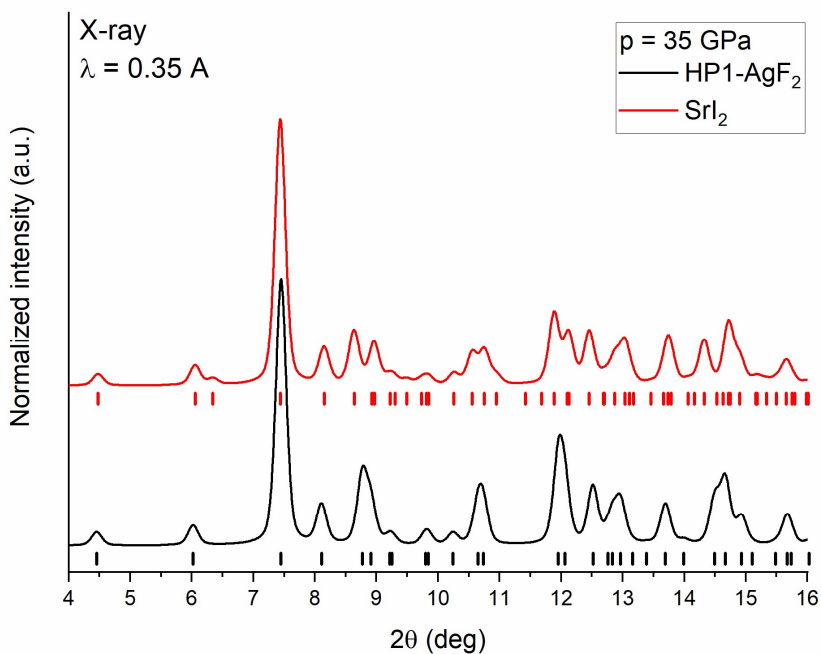


Figure S 6 Comparison of the x-ray diffraction pattern simulated for HP1-AgF_2 and SrI_2 structures optimized at 35 GPa. Vertical lines indicate position of Bragg peaks.

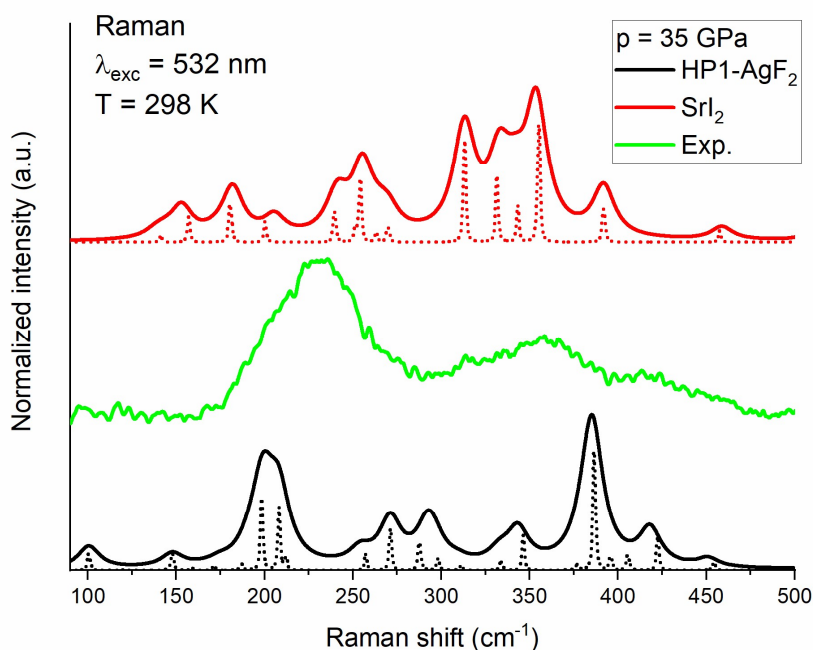


Figure S 7 Comparison of the Raman spectrum simulated for HP1-AgF₂ and SrI₂ optimized at 35 GPa. Full lines indicate the spectrum simulated with a Lorentzian profile with a FWHM of 15 cm⁻¹. The dotted lines correspond to profiles with FWHM equal to 1 cm⁻¹.

Calculated crystal structure of the HP1-AgF2 polymorph of ZnF2 at 35 GPa (in VASP format).

HP1_AgF2 polymorph of ZnF2

```

1.0000000000000000
4.6209453324633118 0.0000000000000000 0.0000000000000000
0.0000000000000000 4.5857984157842093 0.0000000000000000
0.0000000000000000 0.0000000000000000 4.8642234913989029

```

```

Zn F
4 8

```

Direct

```

0.9752991177817992 0.9913420485212134 0.9861618137091862
0.9752991177817992 0.5286580094787874 0.4861618287091768
0.4752991177817992 0.9913420485212134 0.5632781472908183
0.4752991177817992 0.5286580094787874 0.0632781312908169
0.3985438579427227 0.3697360649243133 0.4234472323536149
0.7007269092754664 0.6849133546709573 0.7527392489136677
0.7007269092754664 0.8350866893290424 0.2527392739136663
0.3985438579427227 0.1502639040756837 0.9234472323536149
0.8985438329427171 0.1502639040756837 0.6259927426463907
0.2007269472754695 0.8350866893290424 0.2967007760863349
0.2007269472754695 0.6849133546709573 0.7967007760863349
0.8985438329427171 0.3697360649243133 0.1259927926463877

```